Research Square

Preprints are preliminary reports that have not undergone peer review.
They should not be considered conclusive, used to inform clinical practice,
or referenced by the media as validated information.

Novel Antifungal Compound Z247611722 Exhibits Antifungal Activity by Inhibiting Serine Palmitoyltransferase

Jana Nysten
KU Leuven https://orcid.org/0000-0001-5591-0595
Wout Van Eynde
KU Leuven https://orcid.org/0000-0001-9426-862X
Yunjin Lee
University of Toronto
Eliane Vanhoffelen
KU Leuven
Tine Van Win
KU Leuven https://orcid.org/0009-0001-0657-1328
Greetje Vande Velde
KU Leuven - University of Leuven https://orcid.org/0000-0002-5633-3993
Arnout Voet
University of Leuven
Nicole Robbins
University of Toronto https://orcid.org/0000-0003-2821-9269
Leah Cowen
University of Toronto https://orcid.org/0000-0001-5797-0110
Patrick Van Dijck
patrick.vandijck@kuleuven.be

KU Leuven https://orcid.org/0000-0002-1542-897X

Article

Keywords:

Posted Date: June 18th, 2025

DOI: https://doi.org/10.21203/rs.3.rs-6810020/v1

License: This work is licensed under a Creative Commons Attribution 4.0 International License.
Read Full License

Additional Declarations: Yes there is potential Competing Interest. L.E.C. is a co-founder and shareholder in Bright Angel Therapeutics, a platform company for the development of novel antifungal therapeutics. L.E.C. is a science advisor for Kapoose Creek, a company that harnesses the therapeutic potential of fungi.

Version of Record: A version of this preprint was published at Nature Communications on September 15th, 2026. See the published version at https://doi.org/10.1038/s41467-026-77817-1.

Abstract

The global rise in fungal infections, driven by expanding at-risk populations and growing antifungal resistance, highlights the need for new therapies. However, the current antifungal arsenal remains limited and emerging resistance reduces treatment efficacy. Through high-throughput screening of 20,000 drug-like compounds, we identified Z247611722, a novel fungicidal compound active against multiple *Candida* species and fluconazole-resistant isolates. Chemogenomic, metabolomic, and phenotypic analyses revealed that Z247611722 disrupts sphingolipid biosynthesis, likely by targeting the serine palmitoyltransferase. The mode of action was confirmed by experimental evolution, yielding a resistant strain with a non-synonymous mutation in the serine palmitoyltransferase encoding gene, *LCB2*. Structural docking suggests that Z247611722 interferes with the PLP-binding site, distinguishing its mechanism from known inhibitors such as myriocin. Importantly, Z247611722 demonstrates *in vivo* efficacy in an invertebrate model of *C. albicans* infection. These findings validate Lcb2 as a promising target and introduce a structurally-distinct sphingolipid biosynthesis inhibitor with therapeutic potential.

Introduction

Fungi represent one of the most poorly understood and least studied classes of microorganisms that infect humans[1]. Nevertheless, it is evident that fungal diseases have a significant impact on human health, with over one billion individuals affected and more than 3.8 million attributable deaths annually[2,3]. Approximately one-third of these deaths can be attributed to different *Candida* species, with *Candida albicans, Candida glabrata* (also known as *Nakaseomyces glabratus*), *Candida parapsilosis, Candida tropicalis*, *Candida krusei* (also known as *Pichia kudriavzevii*) and *Candida auris* (also known as *Candidozyma auris*) representing the most prevalent species[2,4]. Nevertheless, due to the historical neglect of fungi, there is a scarcity of antifungal drugs available to treat infections. In response to this pervasive and systemic negligence, the World Health Organization has recently created a priority list for fungal pathogens to address the imbalance between high mortality rates, the upcoming drug resistance crisis, and limited funding. This list aims to systematically prioritize fungal pathogens based on their unmet research and development needs. In this list, *C. albicans* is indicated as a pathogen of critical concern to public health that requires immediate attention[5]. It is a leading cause of nosocomial infections, with an approximate mortality rate of 64%[2]. The current antifungal drug pipeline is limited, encompassing merely three major classes of drugs designated for the treatment of life-threatening invasive fungal infections[6]. In recent years, a small number of improved or novel drugs have entered clinical trials, some of which have already been approved for certain applications[7,8]. However, the scarcity of antifungal drug classes is particularly worrisome considering the escalating crisis of antifungal drug resistance. It is noteworthy that certain *Candida* species exhibit inherent resistance to azoles, a widely used class of antifungal drugs in clinical settings[9]. Moreover, some species demonstrate an enhanced capacity to acquire resistance to commonly utilized medications such as fluconazole, caspofungin, and amphotericin B[9–12]. Alarmingly, resistance to all three major drug classes has now been observed in most human-pathogenic fungi[12]. These trends highlight the pressing need for

drugs with novel modes of action[13]. This is challenging as many core processes and pathways are conserved between fungi and humans, as both are eukaryotes. Consequently, host toxicity is one of the main hurdles when developing antifungal drugs[6].

In this manuscript, we present a newly identified compound that exhibits potent antifungal activity *in vitro* and *in vivo*. This compound was discovered in a high-throughput screen and possesses novel fungicidal activity against various *Candida* species, against a fluconazole-resistant strain, and acts synergistically with fluconazole. Utilizing a multifaceted approach encompassing chemogenomic profiling, alongside metabolomic and phenotypic analyses, it was elucidated that the compound in question disrupts sphingolipid biosynthesis by targeting serine palmitoyltransferase (SPT). Experimental evolution was utilized to generate a resistant strain to validate the compound's mode of action. Subsequent sequencing analysis of this strain revealed a single nucleotide polymorphism (SNP) in *LCB2*, which encodes a subunit of the heterodimeric SPT, resulting in an alanine-to-proline substitution. Notably, structural docking studies suggested that the compound operates through a distinct mechanism compared to known SPT inhibitors, such as myriocin, underscoring its novelty and potential as a therapeutic agent. Lastly, the compound effectively eradicated *C. albicans* in an *in vivo Galleria mellonella* model of infection.

Together, these findings validate SPT as a druggable antifungal target and establish Z247611722 as a structurally distinct, novel inhibitor with therapeutic potential.

Results

Compound Z247611722 displays fungicidal activity against multiple Candida species.

To identify antifungal compounds with novel bioactivity, a structurally-diverse library of 20,000 drug-like compounds was screened against a *C. albicans* wild-type strain (SC5314) at 50 μM in a synthetic LoFlo medium. This approach enabled the selection of compounds capable of effectively penetrating the fungal cell wall and membrane, a common challenge in antifungal drug discovery[14]. Following a 24-hour incubation period at 30°C, absorbance was measured and compared to the controls: a positive control consisting of an essential *RIB1* deletion strain incapable of growth[15], and a negative control comprising a wild-type strain grown without compound (Fig. 1A and Supplementary Table 1). Out of 20,000 compounds, 13 reduced *C. albicans* growth by > 75%, representing a 0.065% hit rate. One of these compounds, Z56812898 (indicated with a green circle), was identified as a potent hit with anti-*C. albicans* activity and no previously reported bioactivity.

To further characterize the bioactivity of Z56812898, three structural analogs were obtained from Enamine and evaluated for their anti-*C. albicans* activity using a two-fold broth dilution assay (BDA) to determine their minimum inhibitory concentration (MIC) (Fig. 1B). Among these, analog Z247611722 exhibited the highest potency. As a result, further investigations focused on Z247611722. This compound, identified as N-(1,3-dimethyl-2,4,7-trioxopyrano[2,3-d]pyrimidin-6-yl)-4-fluorobenzamide,

contains an additional fluorine atom in its benzene ring, a structural feature that differentiates it from the original hit compound identified during the screening. This fluorine atom appeared to be crucial for bioactivity or stability, as Z56812908, which has the fluorine at the 2-position of the benzamide ring as opposed to the 4-position, lost all antifungal activity (Fig. 1B and 1C). Interestingly, Z247611722 displayed medium-dependent activity (Fig. 1D); while it remained active in RPMI and SC media, its efficacy was reduced in SC medium with 10% serum, and no activity was observed in YPD medium. The highest activity was observed in SC medium, with an MIC_{80} of 1.56 µM, corresponding to 0.5387 µg/mL. Based on these findings, all subsequent experiments were conducted in SC medium. Subsequently, the compound was tested against fluconazole-tolerant and -resistant strains, CaCi-2 and CaCi-17, respectively (Fig. 1E). CaCi-2 and CaCi-17 were isolated from an HIV-infected patient. The CaCi-2 strain was isolated early in the course of the infection, while the azole-resistant strain was recovered from the same patient after multiple fluconazole treatments[16]. CaCi-17 has increased expression of *MDR1* (a multidrug efflux pump), *CDR1* (a multidrug transporter of the ABC superfamily), and *ERG11* (the lanosterol 14alpha demethylase encoding gene)[16]. Interestingly, we found that Z247611722 effectively inhibits the fluconazole-resistant strain. Next, the spectrum of activity was assessed against a selection of clinically relevant yeast species. The compound demonstrated activity against multiple *Candida* species, including *C. dubliniensis*, *C. parapsilosis*, *C. auris*, and *C. glabrata*. No activity was observed against *Cryptococcus neoformans or Saccharomyces cerevisiae*. Next, fungicidal activity was assessed by spotting the cells of the BDA on YPD agar without compound. Fungicidal activity was observed against several species, including *C. albicans* and *C. glabrata* (Fig. 1F). In addition to these common fungal yeasts, we tested the compound against the filamentous mold *Aspergillus fumigatus* and two bacterial species, *Escherichia coli*, and *Staphylococcus aureus*, but observed no activity (Supplementary Fig. 1A). To determine whether our prioritized compound enhanced the efficacy of commonly used antifungals, we performed dose-response matrix assays. Interestingly, Z247611722 enhanced the activity of fluconazole, with a fractional inhibitory concentration index at 50% growth inhibition ($FICI_{50}$) of 0.375 and an $FICI_{80}$ of 0.5 (Fig. 1G). An FICI ≤ 0.5 in a single well was interpreted as a synergistic interaction between the compounds. An indifferent interaction was observed in combination with caspofungin (Supplementary Fig. 1B).

Given the favourable activity of the compound we noted *in vitro*, we next assessed the compound's *in vivo* potential. To do so, we first evaluated the toxicity of the compound using a *G. mellonella* model. The compound was diluted in PBS to a final DMSO concentration of 4.88%. The larvae were injected with 10 µL of either the compound, the vehicle control (4.88% DMSO), or PBS alone through the last proleg into the hemocoel. Larvae were monitored for 72 hours, and their health status was evaluated based on movement, melanization, and survival (Supplementary Fig. 1C). Due to solubility limitations of the compound in PBS, the highest tested concentration was 25 mg/kg. No signs of toxicity were observed (Fig. 1H). To assess *in vivo* efficacy, larvae were infected with 5×10^4 cells of a bioluminescent *C. albicans* reporter strain. Treatments with the compound, vehicle, or PBS were administered every 24 hours (Fig. 1I). Survival and health status were monitored daily (Supplementary Figs. 1D and 1E), and fungal burden was quantified via *in vivo* bioluminescence imaging (BLI) over five days. The compound

significantly reduced *C. albicans* burden *in vivo* (Fig. 1J). Thus, Z247611722 and related analogs have novel broad spectrum antifungal activity against important fungal pathogens of humans.

Haploinsufficiency profiling identifies the sphingolipid biosynthetic pathway as a potential target of Z247611722

To elucidate the mode of action of compound Z247611722, we performed haploinsufficiency profiling (HIP) using a pooled double-barcoded heterozygous deletion library (DBC) containing essential and non-essential genes covering over 90% of the *C. albicans* genome[17]. This chemical-genetic approach is based on the principle that a genetic reduction in copy number of the gene encoding a compound's target, or in a gene involved in related pathways, will result in hypersensitivity to the compound[18]. In the DBC mutant collection, one allele of each gene is replaced by an *HIS3* selectable marker flanked by strain-specific barcodes used to identify and quantify individual strains in a pooled population[17,19,20]. This library was cultured in the absence and presence of 1.5 μM Z247611722 for 18 hours, a concentration that resulted in 42% growth inhibition of the mutant pool. The pool was grown in triplicate, genomic DNA was extracted, and the upstream and downstream barcodes were PCR amplified and high-throughput sequenced to assess the relative abundance of the barcoded strains. The $\log_2$ (solvent/drug) ratio was plotted, and all hits above a $\log_2$(solvent/drug) ratio of 2 were considered hypersensitive. The full dataset resulting from the HIP is provided in Supplementary Table 2. As a control, fluconazole was included as an antifungal with the well-defined target Erg11, and indeed, the *ERG11/erg11Δ* heterozygous strain was hypersensitive to fluconazole (Supplementary Fig. 2A). For Z247611722, seven heterozygous strains emerged as hypersensitive to the compound (Fig. 2A) and growth curve analysis in the presence and absence of the compound confirmed the hypersensitivity of six out of seven strains. Among these, the heterozygous deletion strains for *LCB1*, *LCB2*, and *FAS1*, genes involved in sphingolipid or fatty-acid biosynthesis, exhibited the greatest sensitivity to the compound (Fig. 2B). HIP was also performed with the model yeast *S. cerevisiae*, as results from the two species are often complementary, strengthening the mechanism of action predictions[21,22]. Pooled cultures of a barcoded heterozygous deletion collection[23] were cultured in the presence and absence of 40 μM of Z247611722 for 48 h, a concentration that achieved 25% growth inhibition of the mutant pool. The genomic DNA was isolated, and the barcodes were PCR amplified and pooled for high-throughput sequencing to detect the relative abundance of each mutant strain. We observed that, similarly to the HIP profile in *C. albicans*, mutants lacking one allele of *LCB1* and *LCB2* were hypersensitive to the compound (Supplementary Fig. 2B).

To further explore how Z247611722 affects lipid homeostasis, the *C. albicans* gene replacement and conditional expression (GRACE) collection was used. Mutants from this collection lack one allele of the gene of interest, while the remaining allele is regulated by a tetracycline-repressible promoter, which can be repressed using the tetracycline analog doxycycline (DOX)[19]. Available strains related to fatty acid and sphingolipid biosynthesis pathways were tested for Z247611722 susceptibility in the presence and absence of DOX. While not all strains displayed hypersensitivity to Z247611722 upon repression of the target gene, we found that transcriptional repression of *LCB1*, *LCB2*, *FAS1*, *FAS2*, *AUR1*, as well as other

genes involved in sphingolipid biosynthesis, showed increased sensitivity to Z247611722 (Fig. 2C and Supplementary Fig. 3). Based on these susceptibility phenotypes, we hypothesized that the compound impacted sphingolipid biosynthesis. To support this model, we repeated the dose-response assays with the sphingolipid biosynthesis inhibitor myriocin, an inhibitor of the serine palmitoyltransferase (SPT), the enzyme that catalyzes the first step in the sphingolipid biosynthesis pathway (Fig. 3A). Notably, the same mutants from the GRACE collection that displayed hypersensitivity to Z247611722 upon transcriptional repression also displayed hypersensitivity to myriocin. Collectively, this genetic data suggests that Z247611722 is a novel inhibitor of sphingolipid biosynthesis.

Z247611722 inhibits serine palmitoyltransferase, the first and rate-limiting step of the sphingolipid biosynthesis pathway.

To further support that Z247611722 targets the sphingolipid biosynthesis pathway, we assessed its bioactivity in dose-response assays with supplemented fatty acids and sphingolipids added to the medium. To establish a basis for comparison, we also performed the supplementation experiment with myriocin and cerulenin, which inhibit SPT and the formation of fatty acids and sterols, respectively[24,25]. As anticipated, the bioactivity of myriocin was mitigated by the supplementation of phytosphingosine. Conversely, cerulenin's bioactivity was mitigated by myristic acid supplementation, as reported in literature[26]. When examining Z247611722, it was observed that its bioactivity disappeared in the presence of phytosphingosine, an intermediate of the sphingolipid biosynthesis pathway, whereas oleic acid and myristic acid supplementation had no effect (Fig. 3B), similar to myriocin. This indicates that phytosphingosine mitigates the effect of Z247611722, implying that the compound acts upstream of phytosphingosine. To more precisely identify the step in the sphingolipid biosynthesis pathway where Z247611722 acts, we supplemented the medium with three components upstream of phytosphingosine (Fig. 3A): palmitoyl-coenzyme A, 3-ketosphinganine, and sphinganine. The results showed that the bioactivity of Z247611722 was mitigated by the presence of the latter two intermediates, while palmitoyl-coenzyme A did not exhibit this effect (Fig. 3C). It is important to note that palmitoyl-CoA is a bulky long-chain acyl-CoA ester, which has been reported to cross lipid bilayers very slowly or not at all[27,28]. A similar outcome was obtained for myriocin, which was expected as it is a known inhibitor of SPT, but not cerulenin (Fig. 3C). Overall, this suggests Z247611722 exerts its effect on the first step of the sphingolipid biosynthesis pathway, at the level of SPT, or perhaps even further upstream. Given our model that Z247611722 and myriocin both inhibit sphingolipid biosynthesis, a checkerboard assay was conducted to evaluate their potential synergistic or additive effects. As shown in Fig. 3D, the assay yielded an $FICI_{80}$ of 0.5, indicating an additive effect between the two compounds. Cerulenin showed an $FICI_{80}$ of 0.75.

To validate the mode of action of Z247611722, a metabolomics approach was employed to ascertain that the pathway is blocked at the level of SPT. Triplicate cultures of *C. albicans* treated with either Z247611722 or vehicle (DMSO) were collected after four hours of growth in SC medium with 2% U-$^{13}C_6$-glucose. The cell pellets were washed, extracted, and stored at -80°C. Mass spectrometry

measurements were performed to quantify relative levels of key metabolites. The analysis revealed a significant depletion of 3-ketosphinganine and sphinganine in the compound-treated samples, intermediates downstream of SPT, while L-serine and glycine levels, intermediates upstream of SPT, exhibited only a slight reduction in the compound-treated condition (Fig. 3E). These observations were further substantiated by U-$^{13}C_6$-glucose tracing (Fig. 3F). In the presence of the compound, a clear block in the conversion to 3-ketosphinganine was observed, along with a modest reduction in L-serine and glycine levels. We hypothesize that the observed decrease in serine synthesis may be a compensatory response to blockages in the pathway, aimed at maintaining flux through upstream steps. Phosphoglyceric acid, a precursor to L-serine, showed no significant change in abundance, suggesting that the pathway is being partially maintained. Alternatively, the disruption of SPT may indirectly impair serine production by depleting or rerouting metabolic resources, which would limit the availability of intermediates for serine biosynthesis. Together, these findings support the conclusion that Z247611722 disrupts sphingolipid biosynthesis at the level of SPT.

Myriocin is known to enhance the expression of genes involved in the biosynthesis and maturation of lipid droplets[29]. Lipid droplets are cellular organelles with a diameter of 0.5 to 1.5 µm, characterized by a neutral lipid core enclosed by a phospholipid monolayer. These organelles store and regulate excess neutral lipids and fatty acids, thereby providing energy to the cell or protecting cells from lipotoxicity[30,31]. To assess the effect of Z247611722 on lipid droplets, we stained the cells with BODIPY™ 493/503, a green, fluorescent dye ideal for lipid droplet staining due to its hydrophobic properties. To establish a basis of comparison, myriocin, cerulenin, cells without treatment, and cells without dye with Z247611722 were added as controls. We observed that Z247611722 produced a phenotype similar to that of myriocin, significantly inducing lipid droplet formation relative to DMSO (Fig. 4A). To quantify the microscopy findings, we employed flow cytometry to measure the fluorescence of a minimum of 10,000 cells, confirming that both myriocin and Z247611722 increase lipid droplet formation. The collective analysis of these data suggests that Z247611722 exerts its effects on lipid homeostasis in a manner analogous to that of myriocin (Fig. 4B).

An alanine-to-proline substitution in Lcb2 was identified in strains that exhibit resistance to Z247611722

To gain more insights into the mode of action of Z247611722, we experimentally evolved *C. albicans*-resistant mutants. This approach was used to identify the mutation(s) that conferred resistance to the compound under the premise that mutations often occur in the compound target[32,33]. To circumvent the selection of efflux-related mutations, we used a parent strain devoid of four pivotal efflux pumps: *MDR1*, *CDR1*, *CDR2*, and *FLU1*[34]. A single colony from this parental strain was subjected to an *in vitro* experimental evolution assay, where it was exposed to gradually increasing compound concentrations. This process yielded multiple lineages of resistant strains, which were subsequently plated on agar plates with compound to facilitate the isolation of individual colonies. It was observed that the resistant

strains exhibited growth at concentrations up to 12 μM Z247611722 on solid medium and displayed MIC_{80} values approximately four-fold higher than the parent strain in liquid dose-response assays (Fig. 5A). Cross-resistance to fluconazole and caspofungin was also assessed to ensure that the observed mutations did not result in nonspecific resistance. No such changes in antifungal susceptibility were detected (Fig. 5A). To further verify that the resistance phenotype was not due to increased efflux, the resistant strains were stained with the fluorescent dye Nile, a reliable method for quantifying efflux activity via flow cytometry[35,36]. No changes in Nile red accumulation were detected, indicating that efflux was not enhanced (Fig. 5B). Given that Z247611722 and myriocin appear to both inhibit sphingolipid biosynthesis, we tested whether the resistant strains exhibited cross-resistance to myriocin using a BDA. However, no increased resistance was observed compared to the parent strain, indicating that the mutations of the resistant strains are unique to Z247611722 (Fig. 5C). The three evolved strains and the parent strain were sequenced to identify mutations in the genes encoding SPT: *LCB1* and *LCB2.* Notably, all three resistant strains harbored a specific heterozygous single nucleotide polymorphism (SNP), which was not observed in the parent strain (Fig. 5D). This mutation involved a guanine-to-cytosine substitution near the end of *LCB2* gene ($LCB2^{G1498C}$), resulting in an alanine-to-proline substitution. While the recurrence of an identical SNP in independently evolved lineages may seem unexpected, codon usage analysis of *C. albicans* shows that this is the only possible single nucleotide substitution that can produce an alanine-to-proline change at this position. To verify that this SNP confers resistance to Z247611722, we introduced this heterozygous SNP into a SC5314 background strain and compared the susceptibility of the SC5314 and the $LCB2^{G1498C}$ strain towards Z247611722 in a BDA. A four-fold increase in resistance was observed in the $LCB2^{G1498C}$ strain, validating that the heterozygous SNP confers resistance to Z247611722 (Fig. 5D).

To investigate the compound's potential binding mode, a homology model of *C. albicans* SPT was built using the *Homo sapiens* SPT heterodimer cryo-EM structure (PDB ID: 7K0L) as the template. An initial ligand pose was obtained by docking the compound into this binding pocket and further refined using a 10 ns molecular dynamics (MD) simulation (Fig. 5E). Our analysis revealed that Z247611722 binds to the same site as the cofactor pyridoxal 5'-phosphate (PLP), suggesting that it competes for occupancy of the PLP-binding pocket. Superimposing the *C. albicans* SPT homology model with the SPT structures from *G. mellonella*, *S. cerevisiae* (PDB ID: 8C82), and *H. sapiens* (PDB ID: 7K0Q) revealed a highly conserved binding pocket, with the shared exception of three residues: Asn193 and Val388 in Lcb1, and Gln231 in Lcb2, which are a glycine, cysteine and a methionine in the mammalian and *S. cerevisiae* SPTs, respectively (Fig. 5F). The substitution of the polar cysteine with an apolar valine near the apolar fluorophenyl moiety increases selectivity and accounts for the observed lack of bioactivity in the *S. cerevisiae* cells and the lack of toxicity in the *G. mellonella* larvae. Finally, we hypothesized that the A500P substitution in Lcb2 identified in the resistant strains and associated with a four-fold reduction in compound activity, alters the dynamics and conformation of the binding pocket. Specifically, the rigid structure of proline restricts rotation around the N–Cα bond, often introducing kinks, bends, or disruptions in α-helices and β-strands, and it can stabilize or destabilize loops in proteins[37–40]. We hypothesized that the A500P substitution affects the positioning or flexibility of the loop adjacent to the

binding pocket, thereby impairing the proper accommodation of the compound's fluorophenyl moiety, leading to increased resistance (Fig. 5G). Overall, these selection experiments provide additional evidence that Z247611722 binds and inhibits Lcb2 function, perturbing sphingolipid biosynthesis in *C. albicans*.

Discussion

Fungal infections present an escalating global health threat, driven in part by the emergence of resistance to the limited antifungal classes. This underscores the urgent need for new drugs with novel mechanisms of action[13]. In this study, we identified a previously unannotated antifungal compound by screening a library of 20,000 drug-like compounds against the fungal pathogen *C. albicans*. Structural analogs of the initial hit were ordered and compared. Among them, compound Z247611722 emerged as the most promising candidate.

Compound Z247611722 showed potent antifungal activity against a range of *Candida* species, such as *C. albicans*, *C. parapsilosis*, *C. auris*, *C. glabrata*, and a fluconazole-resistant strain, CaCi-17, which has increased mRNA levels of *MDR1*, *CDR1*, and *ERG16*[16]. The compound's synergistic interaction with fluconazole underscores its potential for combinatorial therapy, a promising strategy for overcoming antifungal resistance[41]. Myriocin, which also acts synergistically with fluconazole, has been shown to block the membrane localization and activation of Cdr1, thereby increasing the antifungal activity of fluconazole[42]. Importantly, Z247611722 exhibited fungicidal activity against a range of *Candida* species, which is a desirable characteristic for antifungal agents, especially in patients with compromised immune systems who rely heavily on drug treatments to clear infections[43]. Moreover, fungicidal agents may reduce the risk of resistance development compared to fungistatic drugs, which often require prolonged treatment[44]. Beyond its *in vitro* potency, Z247611722 reduced *C. albicans* burden in an *in vivo G. mellonella* infection model without signs of toxicity, suggesting a favorable safety profile.

Chemogenomic profiling, metabolomic, and phenotypic analyses indicate that SPT is the molecular target of Z247611722. SPT catalyzes the first and essential step of the sphingolipid pathway by condensing palmitoyl-CoA and L-serine, and is encoded by *LCB1* and *LCB2*[45,46]. Sphingolipids are essential components of the eukaryotic cell membrane but also serve as signaling molecules that regulate multiple physiological processes such as growth, morphogenesis, apoptosis, and virulence in pathogenic fungi[45,47–49]. Metabolomic analyses revealed a significant reduction in sphingolipid intermediates downstream of SPT, with a clear metabolic block at 3-ketosphinganine confirmed by U-$^{13}C_6$-glucose tracing, supporting SPT inhibition as the primary mechanism of action. These findings also explain why the antifungal activity of Z247611722 was highly dependent on the assay medium. No bioactivity was observed in YPD or SC medium with 10% FBS serum, likely due to the presence of sphingolipids in the media[50]. A similar observation has been reported for myriocin, a known sphingolipid biosynthesis inhibitor, which also exhibited a greater inhibition in a synthetic YNB medium compared to YPD[50]. These findings suggest that sphingolipid availability in the environment modulates the

compound's antifungal efficacy, as further evidenced by supplementation assays with downstream intermediates of the sphingolipid biosynthesis pathway. Given that the compound's bioactivity is mitigated by sphingolipids present in serum, systemic applications may be limited, but topical formulations, for oral, vaginal, or cutaneous candidiasis, represent promising therapeutic avenues that should be further explored.

Additional insights into Z247611722's binding mode came from structural docking studies, which indicated that Z247611722 interferes with the PLP-binding site of SPT. This distinguishes its mode of action from that of myriocin, which binds to the internal aldimine at the active site of SPT where it acts as a competitive inhibitor for L-serine and palmitoyl-CoA[25,51]. Despite targeting the same enzyme, Z247611722 and myriocin act through complementary mechanisms and display additive effects when combined.

To further explore the mode of action of compound Z247611722, we subjected *C. albicans* to experimental evolution in the presence of the compound to select for resistant mutants. This approach led to the identification of a heterozygous single nucleotide polymorphism (SNP) in *LCB2*, resulting in an alanine-to-proline substitution. We hypothesize that this substitution alters the conformation and dynamics of the binding pocket, thereby impairing compound binding and conferring increased resistance.

In summary, compound Z247611722 is a promising antifungal candidate with a novel mode of action targeting sphingolipid biosynthesis via SPT inhibition. Its fungicidal activity, synergy with fluconazole, and *in vivo* efficacy highlight its therapeutic potential, particularly for superficial infections.

Material and methods

Strains and growth conditions

The strains utilized in this study are listed in Supplementary Table 3. The plasmids and primers are summarized in Supplementary Tables 4 and 5, respectively.

The standard growth conditions used in this study is 30°C in SC medium, which consists of 0.19% yeast nitrogen base without amino acids (Formedium), 0.079% complete supplement mixture (MP Biomedicals), and 2% glucose. The pH was adjusted to 5.5. Other media used are RPMI, which consists of 1.04% RPMI 164 (Thermo Fisher Scientific), 3.453% MOPS at pH 7, and LoFlo medium, which consists of 0.19% yeast nitrogen base without amino acids, folic acid, and riboflavin (Formedium), 0.079% complete supplement mixture (MP Biomedicals), and 2% glucose. The pH of the latter medium was adjusted to 5.5.

High-throughput screening of 20,000 drug-like molecules

A drug-like compound library of 20,000 molecules, acquired from Enamine and available through the VIB screening core Ghent was screened at 50 µM against *C. albicans* SC5314 in LoFlo medium at 30°C.

Overnight cultures of SC5314 and *rib1Δ/Δ* (positive control) were washed 3 times in LoFlo and were subsequently diluted to OD_{600} 0.1 in 384 well plates. Compound or DMSO was added to the plates using an echo acoustic dispenser. The plates were incubated for 24 hours at 30°C with shaking before measuring the OD_{600}.

Susceptibility testing

Two-fold BDA assays were conducted using 96-well or 384-well plates, incubated at 30°C in the dark under static conditions. Overnight cultures were diluted to 2 × 10^3 cells per well, and two-fold compound dilutions were added to the plates. Absorbance at 600 nm was measured at specified time points using a spectrophotometer (Molecular Devices).

For the GRACE collection (*tetO* mutants), strains were grown overnight with and without doxycycline (DOX) to induce transcriptional repression. DOX was used at 0.05 µg/mL for essential genes and at 20 µg/mL for non-essential genes, with these concentrations maintained throughout the experiment.

In assays involving (sphingo)lipid supplementation, the lipids were dissolved in DMSO and diluted into SC medium containing *C. albicans*, following the concentrations specified in the results section. The cidality of the compounds was assessed by stamping the cultures onto compound-free YPD agar plates.

Data analysis involved subtracting the blank medium values, averaging technical replicates, and normalizing the data to the no-drug control. Relative growth was represented in heat maps.

Toxicity and efficacy tests in Galleria mellonella

Galleria mellonella larvae were bred in-house and healthy 6th -instar larvae of 300 ± 50 mg were randomly selected and sorted into groups of 10 for experiments. After infection, the larvae were housed individually in 12-well plates, in the dark without food at 37°C.

For toxicity assays, larvae were injected with 10 µL of compound or vehicle through the last proleg into the hemocoel using a Hamilton syringe (model 701SN, 31 gauge; Hamilton Company, Switzerland) and monitored for 72h. The health was scored by assessing the movement, melanization, and survival, similar to what was previously described by Vanhoffelen et al.[52].

For efficacy studies, larvae were first injected with 10 µL of bioluminescent *C. albicans* reporter strain[53] in the last proleg, and one hour later, the compound or vehicle was injected. The compound or vehicle was injected every 24 hours for five days. Larval health was monitored daily, and the fungal load was assessed daily with BLI using an IVIS Spectrum imaging system (Revvity). 10 µL of 40 µg/g D-Luciferin was injected into the hemocoel prior to every imaging session and the larvae were transferred to a black 12-well plate with a transparent bottom (IBL Baustoff + Labor GmbH, Austria) at 37°C for 10 min[52,54,55]. Bioluminescence emission was measured by capturing five consecutive images using the following settings: open filter, F/stop 1, subject height 0.5 cm, medium binning, and a 30 s exposure time per

image. Total photon flux (p/s) per larva was quantified using Living Image Software (version 4.5.4) by defining a circular region of interest (ROI) with a 2.5 cm diameter covering each well.

Haploinsufficiency profiling in C. albicans

A glycerol aliquot of the *C. albicans* double-barcoded pool of heterozygous deletion mutants was thawed and diluted to OD_{600} 0.05 in triplicate in SC medium. These cultures were incubated at 30°C with shaking for 90 minutes. Each culture was then diluted two-fold into 5 mL SC medium, with and without compound, and incubated under the same conditions for 18 hours. Cells were harvested by centrifugation, and the pellets were stored at − 80°C.

Samples were prepared for barcode sequencing following previously described methods[20]. Equal amounts of UP-TAG and DOWN-TAG pools were combined to create a sequencing library, which was run on an Illumina NextSeq500 platform (Mid-Output, V2 Chemistry). Specific primers were used for sequencing and indexing UP-TAGs and DOWN-TAGs. Barcode sequences were mapped to an artificial genome of known UP-TAG and DOWN-TAG sequences using Bowtie v1.0 (http://bowtie-bio.sourceforge.net/index.shtml). Read frequencies for each strain's UP-TAG and DOWN-TAG were compiled for all indexed samples. UP-TAGs or DOWN-TAGs where more than one triplicate sample had solvent-only read counts below 20% of the median per million mapped reads were excluded from further analysis. Log_2-fold differences were calculated for each strain's UP-TAG and DOWN-TAG.

Haploinsufficiency profiling in S. cerevisiae

The pooled heterozygous diploid mutant library was aliquoted into 96-well plates containing SC medium with the test compound at the concentration specified in the results section. After 48 hours of static growth at 30°C, OD600 was measured, and percentage growth inhibition was calculated. Technical replicates were pooled, and the cells were harvested by centrifugation and stored at − 80°C. Genomic DNA was subsequently extracted, and strain-specific barcodes were amplified using barcode PCR. The samples were sent for sequencing, and the data were analyzed using the BEAN-counter software pipeline[56]. Strains with fewer than 20 barcode read counts were excluded from further analysis.

HIP validation growth curves

Heterozygous deletion strains and the HIP parent strain were cultured overnight and subsequently diluted to 2 × 10^3 cells per well in 384-well plates containing SC medium, in the presence or absence of the compound. Similarly to the HIP, we aimed for growth inhibition of 15–30% in the presence of compound. Plates were grown at 30°C while shaking. The $absorbance_{600}$ was measured every 30 minutes using the Tecan Infinite 200 Pro. The ratio of the AUC with and without compound was determined and normalized to the ratio of the AUC of the parental strain. The mean of three technical replicates is shown.

Lipid droplet assay

C. albicans was cultured overnight in SC medium. The cells were subcultured to an OD_{600} of 0.1 in fresh SC medium and grown for 2 hours at 30°C. Following this, compounds were added to the cultures, and the cells were incubated for an additional 4 hours. The cells were then stained with 1 µg/mL BODIPY 493/503 for 10 minutes, collected by centrifugation, and washed three times with PBS. The samples were visualized using a Zeiss Axio Imager.MI microscope at 100× magnification with an enhanced GFP (EGFP) filter and DIC.

To quantify relative lipid droplet volumes, flow cytometry was performed using the FITC (488 nm) channel. Debris was excluded by gating based on forward versus side scatter, with a minimum of 10,000 events included in the analysis.

Metabolomics

An overnight culture of SC5314 in SC medium was washed three times with PBS and the OD_{600} was adjusted to 1 in 2 mL test tube of SC medium. After 2 hours of incubation at 30°C, Z247611722 was added to three test tubes to a final concentration of 16 µM. DMSO was added to the control tubes. The tubes were incubated for an additional hour prior to spinning down all the cells and transferring them into a fresh test tube containing SC medium with 2% U-$^{13}C_6$-glucose, and 16 µM Z247611722 or DMSO to the control tubes. After 4 hours of incubation, The OD_{600} was measured and the cells were spun down in and kept on ice. The medium was removed and 1mL of cold washing buffer (0,9% NaCl dissolved in MilliQ water) was added. The cells were spun down and the washing solution was removed and 300 µL ice-cold extraction buffer was added to the tubes. This mixture was vortexed and stored at -80°C.

Mass Spectrometry measurements were performed using Dionex UltiMate 3000 LC System (Thermo Scientific) coupled to a Q Exactive Orbitrap mass spectrometer (Thermo Scientific) operated in positive mode. 10 µl sample was injected into a Poroshell 120 HILIC-Z PEEK Column (Agilent InfinityLab). A linear gradient was carried out starting with 90% solvent A (acetonitrile) and 10% solvent B (10 mM Na-acetate in mqH2O, pH 9.3). From 2 to 12 min the gradient changed to 60% B. The gradient was kept on 60% B for 3 minutes and followed by a decrease to 10% B. The chromatography was stopped at 25 min. The flow was kept constant at 0.25 ml/min. The column's temperature was kept constant at 25 degrees Celsius. The mass spectrometer operated in full scan (range [70.0000-1050.0000]) and positive mode using a spray voltage of 3 kV, capillary temperature of 320°C, sheath gas at 45, and auxiliary gas at 10. AGC target was set at 3.0E + 006 using a resolution of 70000. Data collection was performed using the Xcalibur software (Thermo Scientific). The data analyses were performed by integrating the peak areas (El-Maven – Polly - Elucidata)

Experimental evolution assay

To generate resistant mutants to Z247611722, five independent lineages of *mdr1Δ/Δ cdr1Δ/Δ cdr2Δ/Δ flu1Δ/Δ* strain were cultured in 5 mL SC medium in the presence of compound starting with a

concentration of 0.78 µM (0.5 x MIC50). After 24 hours of incubation at 30°C under shaking conditions, growth was compared to the compound-free condition by measuring OD_{600}. When the OD_{600} of the compound-treated samples were half of the control samples without compound, the cells were collected by centrifugation and the amount of compound was doubled until the cells were able to grow at 100 µM of compound. When the cells did not reach this OD_{600}, they were incubated for an additional 24h. When resistant strains were made, the cells were restreaked on SC agar plates with compound to obtain single colonies. Single colonies were grown overnight in SC medium without compound and tested in BDAs with the parental strain. Strains that showed resistance were sequenced.

Nile red accumulation assays were performed to exclude that the strains were resistant through the upregulation of drug efflux pumps. This assay was previously described by Iyer et al.[36].

Heterozygous SNP construction in SC5314 background

The heterozygous SNP was created using the *SAT1* flipper tool, as described by Reuß et al.[57]. A plasmid with a deletion cassette with homologous regions at the end of the *LCB2* gene was engineered. The forward primer used to create the upstream fragment contained the guanine-to-cytosine substitution. The downstream region was approximately 500 bp long and was immediately adjacent to the upstream fragment as no part of the gene needed to be deleted. These homologous regions were amplified using genomic DNA from the wild-type strain. The backbone utilized was pSFS2n, with ApaI and XhoI restriction enzymes applied for the introduction of the upstream fragment, and NotI and SacI employed to introduce the downstream homologous fragment regions. After extracting the correct Gibson (NEBuilder® HiFi DNA Assembly) ligated plasmid from competent *E. coli* cells, the plasmid was cut using ApaI and SacI and transformed into *C. albicans* wild-type cells with the lithium acetate method[58]. The transformed cells were then plated on YPD plates containing 200 µg/mL nourseothricin (WERNER BIO). Subsequently, the cassette was removed from the genome through FLP-mediated excision. The heterozygous SNP was verified using Sanger sequencing.

Molecular modelling studies

The *Homo sapiens* SPT heterodimer cryo-EM structure (PDB ID: 7K0L) was processed using the QuickPrep module in MOE v.2024.6 (*Molecular Operating Environment (MOE)*, 2024.0601 Chemical Computing Group ULC, 910–1010 Sherbrooke St. W., Montreal, QC H3A 2R7, **2024**.), combining 3D protonation and energy minimization with the AMBER:EHT force field. Subsequently, the *Candida albicans* Lcb1 and Lcb2 sequence (http://www.candidagenome.org/cgi-bin/protein/proteinPage.pl?dbid=CAL0000192873&seq_source=C.%20albicans%20SC5314%20Assembly%2022, http://www.candidagenome.org/cgi-bin/protein/proteinPage.pl?dbid=CAL0000186740&seq_source=C.%20albicans%20SC5314%20Assembly%2022) was modeled onto this *H. sapiens* structure using the myriocin ligand as an induced fit environment. Intermediate models were refined, and the highest-scoring homology model was selected.

Next, molecular docking was performed. The Z247611722 ligand was prepared in its dominant protonation state at pH 7 using the MMFF94x force field, and conformers were generated with the ConfSearch module. These conformers were docked into the binding pocket using the Triangle Matcher placement method and Induced Fit refinement, scored with GBVI/WSA dG. Only the predicted pose was retained.

Before conducting 10 ns molecular dynamics (MD) simulations to stabilize the protein-ligand interactions using GROMACS v.2024.3 [https://doi.org/10.1002/jcc.20291], the system was prepared with the CHARMM-GUI webserver in order to include parameters for the complex [https://doi.org/10.1002/jcc.20945; https://doi.org/10.1021/acs.jctc.5b00935]. This setup included the 4-point OPC rigid water model [https://doi.org/10.1021/jz501780a], the ff19SB force field for proteins [https://doi.org/10.1021/acs.jctc.9b00591], the gaff2 force field for small molecules [https://onlinelibrary.wiley.com/doi/10.1002/jcc.20035], and the 12–6–4 Lennard-Jones potential model for divalent ions [https://doi.org/10.1021/acs.jctc.0c00194].

The complex was centered in a cubic simulation box, maintaining a minimum distance of 1 nm from the box boundaries. The system was solvated with water molecules, neutralized with Cl^- and Na^+ ions reflecting a 0.1 M NaCl concentration within the box, and then energy-minimized using the steepest descent method [https://doi.org/10.3390/math9111197]. Non-bonded interactions were computed with the Verlet cutoff scheme [https://doi.org/10.1016/j.cpc.2013.06.003], and long-range electrostatics were handled using the Particle Mesh Ewald (PME) method [https://doi.org/10.1063/1.464397]. Bond lengths were constrained with the LINCS algorithm [https://doi.org/10.1021/ct700200b]. Following energy minimization, the system was equilibrated to 300 K and a density of 1000 kg/m³. First, a 100-ps equilibration under an NVT ensemble using the V-rescale thermostat was performed, followed by another 100-ps equilibration under an NPT ensemble with the V-rescale thermostat and the C-rescale barostat [https://doi.org/10.1063/1.2408420; https://doi.org/10.1063/5.0020514]. Positional restraints were applied to the complex throughout equilibration. During the production run, pressure control was maintained using the C-rescale barostat and temperature control using the V-rescale thermostat.

After visually inspecting the simulation, its last frame was extracted and post-processed using QuickPrep, applying protonation and energy minimization.

The structure of the mammalian SPT from *G. mellonella* was predicted using the AlphaFold3 server, based on the amino acid sequences of its Lcb1 and Lcb2 subunits. (https://www.nature.com/articles/s41586-024-07487-w; https://www.uniprot.org/uniprotkb/A0A6J1WZP9/entry#sequences; https://www.ncbi.nlm.nih.gov/protein/XP_052754724.1?report=fasta).

Declarations

Author contributions

Conceptualization: J.N., N.R. L.E.C. and P.V.D.; Formal analysis: J.N. and W.V.E.; Funding Acquisition: J.N., L.E.C, and P.V.D.; Investigation: J.N., W.V.E., E.V., and T.V.W. Methodology: J.N., W.V.E., Y.L., G.V.V., N.R. and L.E.C. Resources: G.V.V., A.V., L.E.C., and P.V.D.; Supervision: A.V., G.V.V., N.R, L.E.C., and P.V.D.; Writing – original draft: J.N. and W.V.E.; All authors edited and/or approved the manuscript.

Acknowledgments

We thank Merck and Genome Canada for making the original GRACE mutant collections available. We acknowledge the excellent support with animal and imaging facilities by Kasia Błażejczyk. J.N. was supported by a PhD fellowship strategic basic research and a travel grant for a long research stay abroad by the Fund for Scientific Research Flanders (1S18121N and V410324N) and by a personal grant from KU Leuven VTI-24-00176. W.V.E. and A.V. were supported by an FWO grant (G0C0222N). E.V. was supported by a PhD fellowship strategic basic research by FWO (1SF2224N). L.E.C. is supported by the Canadian Institutes of Health Research (CIHR) Foundation grant (FDN-154288) and is a Canada Research Chair (Tier 1) in Microbial Genomics & Infectious Disease and co-Director of the CIFAR Fungal Kingdom: Threats & Opportunities program. This work was supported by the KU Leuven Research Council (C14/22/075) to P.V.D. and C3/23/005 to G.V.V..

Declaration of interest

L.E.C. is a co-founder and shareholder in Bright Angel Therapeutics, a platform company for the development of novel antifungal therapeutics. L.E.C. is a science advisor for Kapoose Creek, a company that harnesses the therapeutic potential of fungi.

References

1. Brown, G. D. *et al.* The pathobiology of human fungal infections. *Nat Rev Microbiol*, doi:10.1038/s41579-024-01062-w (2024).
2. Denning, D. W. Global incidence and mortality of severe fungal disease. *Lancet Infect Dis*, doi:10.1016/S1473-3099(23)00692-8 (2024).
3. Bongomin, F., Gago, S., Oladele, R. O. & Denning, D. W. Global and Multi-National Prevalence of Fungal Diseases-Estimate Precision. *J Fungi (Basel)* **3**, doi:10.3390/jof3040057 (2017).
4. Turner, S. A. & Butler, G. The *Candida* pathogenic species complex. *Cold Spring Harb Perspect Med* **4**, a019778, doi:10.1101/cshperspect.a019778 (2014).
5. Burki, T. WHO publish fungal priority pathogens list. *Lancet Microbe* **4**, e74, doi:10.1016/S2666-5247(23)00003-4 (2023).
6. Robbins, N., Wright, G. D. & Cowen, L. E. Antifungal Drugs: The Current Armamentarium and Development of New Agents. *Microbiol Spectr* **4**, doi:10.1128/microbiolspec.FUNK-0002-2016 (2016).
7. Wolfgruber, S., Salmanton-Garcia, J., Kuate, M. P. N., Hoenigl, M. & Brunelli, J. G. P. Antifungal pipeline: New tools for the treatment of mycoses. *Rev Iberoam Micol* **41**, 68-78,

doi:10.1016/j.riam.2024.11.001 (2024).

8. Johnson, M. D. & Moore, W. J. Current Antifungals and the Developing Pipeline. *Infect Dis Clin North Am*, doi:10.1016/j.idc.2025.01.001 (2025).
9. Vale-Silva, L. A. & Sanglard, D. Tipping the balance both ways: drug resistance and virulence in *Candida glabrata*. *FEMS Yeast Res* **15**, fov025, doi:10.1093/femsyr/fov025 (2015).
10. Deorukhkar, S. C., Saini, S. & Mathew, S. Non-*albicans Candida* Infection: An Emerging Threat. *Interdiscip Perspect Infect Dis* **2014**, 615958, doi:10.1155/2014/615958 (2014).
11. Carolus, H. *et al.* Genome-Wide Analysis of Experimentally Evolved *Candida auris* Reveals Multiple Novel Mechanisms of Multidrug Resistance. *mBio* **12**, doi:10.1128/mBio.03333-20 (2021).
12. Berman, J. & Krysan, D. J. Drug resistance and tolerance in fungi. *Nat Rev Microbiol* **18**, 319-331, doi:10.1038/s41579-019-0322-2 (2020).
13. Krysan, D. J. The unmet clinical need of novel antifungal drugs. *Virulence* **8**, 135-137, doi:10.1080/21505594.2016.1276692 (2017).
14. Perfect, J. R. The antifungal pipeline: a reality check. *Nat Rev Drug Discov* **16**, 603-616, doi:10.1038/nrd.2017.46 (2017).
15. 15 Nysten, J. *et al.* The riboflavin biosynthetic pathway as a novel target for antifungal drugs against *Candida* species. *mBio* **15**, e0250224, doi:10.1128/mbio.02502-24 (2024).
16. White, T. C. Increased mRNA levels of *ERG16*, *CDR*, and *MDR1* correlate with increases in azole resistance in *Candida albicans* isolates from a patient infected with human immunodeficiency virus. *Antimicrob Agents Chemother* **41**, 1482-1487, doi:10.1128/AAC.41.7.1482 (1997).
17. Xu, D. *et al.* Genome-wide fitness test and mechanism-of-action studies of inhibitory compounds in *Candida albicans*. *PLoS Pathog* **3**, e92, doi:10.1371/journal.ppat.0030092 (2007).
18. Robbins, N. & Cowen, L. E. Genomic Approaches to Antifungal Drug Target Identification and Validation. *Annu Rev Microbiol* **76**, 369-388, doi:10.1146/annurev-micro-041020-094524 (2022).
19. Roemer, T. *et al.* Large-scale essential gene identification in *Candida albicans* and applications to antifungal drug discovery. *Mol Microbiol* **50**, 167-181, doi:10.1046/j.1365-2958.2003.03697.x (2003).
20. Robbins, N., Ketela, T., Kim, S. H. & Cowen, L. E. Chemical-Genetic Approaches for Exploring Mode of Action of Antifungal Compounds in the Fungal Pathogen *Candida albicans*. *Methods Mol Biol* **2658**, 145-165, doi:10.1007/978-1-0716-3155-3_10 (2023).
21. Fu, C. *et al.* Leveraging machine learning essentiality predictions and chemogenomic interactions to identify antifungal targets. *Nat Commun* **12**, 6497, doi:10.1038/s41467-021-26850-3 (2021).
22. Iyer, K. R. *et al.* Identification of triazenyl indoles as inhibitors of fungal fatty acid biosynthesis with broad-spectrum activity. *Cell Chem Biol* **30**, 795-810 e798, doi:10.1016/j.chembiol.2023.06.005 (2023).
23. Piotrowski, J. S. *et al.* Functional annotation of chemical libraries across diverse biological processes. *Nat Chem Biol* **13**, 982-993, doi:10.1038/nchembio.2436 (2017).

24. Nomura, S., Horiuchi, T., Omura, S. & Hata, T. The action mechanism of cerulenin. I. Effect of cerulenin on sterol and fatty acid biosynthesis in yeast. *J Biochem* **71**, 783-796, doi:10.1093/oxfordjournals.jbchem.a129827 (1972).
25. Wadsworth, J. M. *et al.* The chemical basis of serine palmitoyltransferase inhibition by myriocin. *J Am Chem Soc* **135**, 14276-14285, doi:10.1021/ja4059876 (2013).
26. Awaya, J., Ohno, T., Ohno, H. & Omura, S. Substitution of cellular fatty acids in yeast cells by the antibiotic cerulenin and exogenous fatty acids. *Biochim Biophys Acta* **409**, 267-273, doi:10.1016/0005-2760(75)90022-3 (1975).
27. Asciolla, J. J. & Resh, M. D. Hedgehog Acyltransferase Promotes Uptake of Palmitoyl-CoA across the Endoplasmic Reticulum Membrane. *Cell Rep* **29**, 4608-4619 e4604, doi:10.1016/j.celrep.2019.11.110 (2019).
28. Bavdek, A., Vazquez, H. M. & Conzelmann, A. Enzyme-coupled assays for flip-flop of acyl-Coenzyme A in liposomes. *Biochim Biophys Acta* **1848**, 2960-2966, doi:10.1016/j.bbamem.2015.08.020 (2015).
29. Signorelli, P. *et al.* Myriocin modulates the altered lipid metabolism and storage in cystic fibrosis. *Cell Signal* **81**, 109928, doi:10.1016/j.cellsig.2021.109928 (2021).
30. Wang, C. W. Lipid droplet dynamics in budding yeast. *Cell Mol Life Sci* **72**, 2677-2695, doi:10.1007/s00018-015-1903-5 (2015).
31. Tauchi-Sato, K., Ozeki, S., Houjou, T., Taguchi, R. & Fujimoto, T. The surface of lipid droplets is a phospholipid monolayer with a unique Fatty Acid composition. *J Biol Chem* **277**, 44507-44512, doi:10.1074/jbc.M207712200 (2002).
32. 32 Cowen, L. E. *et al.* Evolution of drug resistance in experimental populations of Candida albicans. *J Bacteriol* **182**, 1515-1522, doi:10.1128/JB.182.6.1515-1522.2000 (2000).
33. Huang, M., McClellan, M., Berman, J. & Kao, K. C. Evolutionary dynamics of Candida albicans during in vitro evolution. *Eukaryot Cell* **10**, 1413-1421, doi:10.1128/EC.05168-11 (2011).
34. Calabrese, D., Bille, J. & Sanglard, D. A novel multidrug efflux transporter gene of the major facilitator superfamily from Candida albicans (FLU1) conferring resistance to fluconazole. *Microbiology (Reading)* **146 (Pt 11)**, 2743-2754, doi:10.1099/00221287-146-11-2743 (2000).
35. Ivnitski-Steele, I. *et al.* Identification of Nile red as a fluorescent substrate of the *Candida albicans* ATP-binding cassette transporters Cdr1p and Cdr2p and the major facilitator superfamily transporter Mdr1p. *Anal Biochem* **394**, 87-91, doi:10.1016/j.ab.2009.07.001 (2009).
36. Iyer, K. R., Robbins, N. & Cowen, L. E. Flow Cytometric Measurement of Efflux in *Candida* Species. *Curr Protoc Microbiol* **59**, e121, doi:10.1002/cpmc.121 (2020).
37. Pavlicek, J. *et al.* Evidence that proline focuses movement of the floppy loop of arylalkylamine N-acetyltransferase (EC 2.3.1.87). *J Biol Chem* **283**, 14552-14558, doi:10.1074/jbc.M800593200 (2008).
38. 38 Nam, G. H. *et al.* The conserved cis-Pro39 residue plays a crucial role in the proper positioning of the catalytic base Asp38 in ketosteroid isomerase from Comamonas testosteroni. *Biochem J* **375**, 297-305, doi:10.1042/BJ20030263 (2003).

39. Ramaswamy, S., Park, D. H. & Plapp, B. V. Substitutions in a flexible loop of horse liver alcohol dehydrogenase hinder the conformational change and unmask hydrogen transfer. *Biochemistry* **38**, 13951-13959, doi:10.1021/bi991731i (1999).
40. Sun, Z. & Liu, J. N. Mutagenesis at Pro309 of single-chain urokinase-type plasminogen activator alters its catalytic properties. *Proteins* **61**, 870-877, doi:10.1002/prot.20686 (2005).
41. Spitzer, M., Robbins, N. & Wright, G. D. Combinatorial strategies for combating invasive fungal infections. *Virulence* **8**, 169-185, doi:10.1080/21505594.2016.1196300 (2017).
42. Wang, H. *et al.* Myriocin enhances the antifungal activity of fluconazole by blocking the membrane localization of the efflux pump Cdr1. *Front Pharmacol* **13**, 1101553, doi:10.3389/fphar.2022.1101553 (2022).
43. Beattie, S. R. & Krysan, D. J. Antifungal drug screening: thinking outside the box to identify novel antifungal scaffolds. *Curr Opin Microbiol* **57**, 1-6, doi:10.1016/j.mib.2020.03.005 (2020).
44. Zavrel, M., Esquivel, B.D., White, T.C. The Ins and Outs of Azole Antifungal Drug Resistance: Molecular Mechanisms of Transport. *Handbook of Antimicrobial Resistance. Springer*, doi:https://doi.org/10.1007/978-1-4939-0694-9_29 (2017).
45. McEvoy, K., Normile, T. G. & Del Poeta, M. Antifungal Drug Development: Targeting the Fungal Sphingolipid Pathway. *J Fungi (Basel)* **6**, doi:10.3390/jof6030142 (2020).
46. 46 Tafesse, F. G. *et al.* Disruption of Sphingolipid Biosynthesis Blocks Phagocytosis of *Candida albicans*. *PLoS Pathog* **11**, e1005188, doi:10.1371/journal.ppat.1005188 (2015).
47. Oura, T. & Kajiwara, S. *Candida albicans* sphingolipid C9-methyltransferase is involved in hyphal elongation. *Microbiology (Reading)* **156**, 1234-1243, doi:10.1099/mic.0.033985-0 (2010).
48. Rouabhia, M. *et al.* Disruption of sphingolipid biosynthetic gene *IPT1* reduces *Candida albicans* adhesion and prevents activation of human gingival epithelial cell innate immune defense. *Med Mycol* **49**, 458-466, doi:10.3109/13693786.2010.535031 (2011).
49. Luberto, C. *et al.* Roles for inositol-phosphoryl ceramide synthase 1 (IPC1) in pathogenesis of *C. neoformans*. *Genes Dev* **15**, 201-212, doi:10.1101/gad.856001 (2001).
50. Mahto, K. K. *et al.* An assessment of growth media enrichment on lipid metabolome and the concurrent phenotypic properties of *Candida albicans*. *PLoS One* **9**, e113664, doi:10.1371/journal.pone.0113664 (2014).
51. Yu, L. *et al.* Theoretical study of myriocin-binding mechanism targeting serine palmitoyltransferase. *Chem Biol Drug Des* **99**, 373-381, doi:10.1111/cbdd.13991 (2022).
52. 52 Vanhoffelen, E. *et al.* Powerful and Real-Time Quantification of Antifungal Efficacy against Triazole-Resistant and -Susceptible *Aspergillus fumigatus* Infections in *Galleria mellonella* by Longitudinal Bioluminescence Imaging. *Microbiol Spectr* **11**, e0082523, doi:10.1128/spectrum.00825-23 (2023).
53. Jacobsen, I. D., Luttich, A., Kurzai, O., Hube, B. & Brock, M. In vivo imaging of disseminated murine *Candida albicans* infection reveals unexpected host sites of fungal persistence during antifungal therapy. *J Antimicrob Chemother* **69**, 2785-2796, doi:10.1093/jac/dku198 (2014).

54. 54 Vanhoffelen, E. *et al.* Combinations of posaconazole and tacrolimus are effective against infections with azole-resistant Aspergillus fumigatus. *Front Cell Infect Microbiol* **15**, 1550457, doi:10.3389/fcimb.2025.1550457 (2025).
55. Vanhoffelen, E. *et al.* Sensitive bioluminescence imaging of cryptococcosis in Galleria mellonella improves antifungal screening under in vivo conditions. *Virulence* **15**, 2327883, doi:10.1080/21505594.2024.2327883 (2024).
56. Simpkins, S. W., Deshpande, R., Nelson, J. et al. Using BEAN-counter to quantify genetic interactions from multiplexed barcode sequencing experiments. *Nat Protoc* **14**, doi:https://doi.org/10.1038/s41596-018-0099-1 (2019).
57. Reuß, O., Vik, A., Kolter, R. & Morschhäuser, J. The *SAT1* flipper, an optimized tool for gene disruption in *Candida albicans*. *Gene* **341**, 119-127, doi:10.1016/j.gene.2004.06.021 (2004).
58. Gietz, R. D. & Schiestl, R. H. High-efficiency yeast transformation using the LiAc/SS carrier DNA/PEG method. *Nat Protoc* **2**, 31-34, doi:10.1038/nprot.2007.13 (2007).
59. Gillum, A. M., Tsay, E. Y. & Kirsch, D. R. Isolation of the *Candida albicans* gene for orotidine-5'-phosphate decarboxylase by complementation of *S. cerevisiae* ura3 and *E. coli* pyrF mutations. *Mol Gen Genet* **198**, 179-182, doi:10.1007/BF00328721 (1984).
60. Suzuki, Y. *et al.* Knocking out multigene redundancies via cycles of sexual assortment and fluorescence selection. *Nat Methods* **8**, 159-164, doi:10.1038/nmeth.1550 (2011).
61. White, T. C. The presence of an R467K amino acid substitution and loss of allelic variation correlate with an azole-resistant lanosterol 14alpha demethylase in *Candida albicans*. *Antimicrob Agents Chemother* **41**, 1488-1494, doi:10.1128/AAC.41.7.1488 (1997).
62. Sullivan, D. J., Westerneng, T. J., Haynes, K. A., Bennett, D. E. & Coleman, D. C. *Candida dubliniensis* sp. nov.: phenotypic and molecular characterization of a novel species associated with oral candidosis in HIV-infected individuals. *Microbiology (Reading)* **141 (Pt 7)**, 1507-1521, doi:10.1099/13500872-141-7-1507 (1995).
63. Lockhart, S. R. *et al.* Simultaneous Emergence of Multidrug-Resistant *Candida auris* on 3 Continents Confirmed by Whole-Genome Sequencing and Epidemiological Analyses. *Clin Infect Dis* **64**, 134-140, doi:10.1093/cid/ciw691 (2017).
64. Lutgring, J. D. *et al.* FDA-CDC Antimicrobial Resistance Isolate Bank: a Publicly Available Resource To Support Research, Development, and Regulatory Requirements. *J Clin Microbiol* **56**, doi:10.1128/JCM.01415-17 (2018).
65. Cormack, B. P. & Falkow, S. Efficient homologous and illegitimate recombination in the opportunistic yeast pathogen *Candida glabrata*. *Genetics* **151**, 979-987, doi:10.1093/genetics/151.3.979 (1999).
66. Granger, D. L., Perfect, J. R. & Durack, D. T. Virulence of *Cryptococcus neoformans*. Regulation of capsule synthesis by carbon dioxide. *J Clin Invest* **76**, 508-516, doi:10.1172/JCI112000 (1985).
67. 67 Polvi, E. J. *et al.* Functional divergence of a global regulatory complex governing fungal filamentation. *PLoS Genet* **15**, e1007901, doi:10.1371/journal.pgen.1007901 (2019).

68. Stone, S. D., Lajkiewicz, N. J., Whitesell, L., Hilmy, A. & Porco, J. A., Jr. Biomimetic kinetic resolution: highly enantio- and diastereoselective transfer hydrogenation of aglain ketones to access flavagline natural products. *J Am Chem Soc* **137**, 525-530, doi:10.1021/ja511728b (2015).

Figures

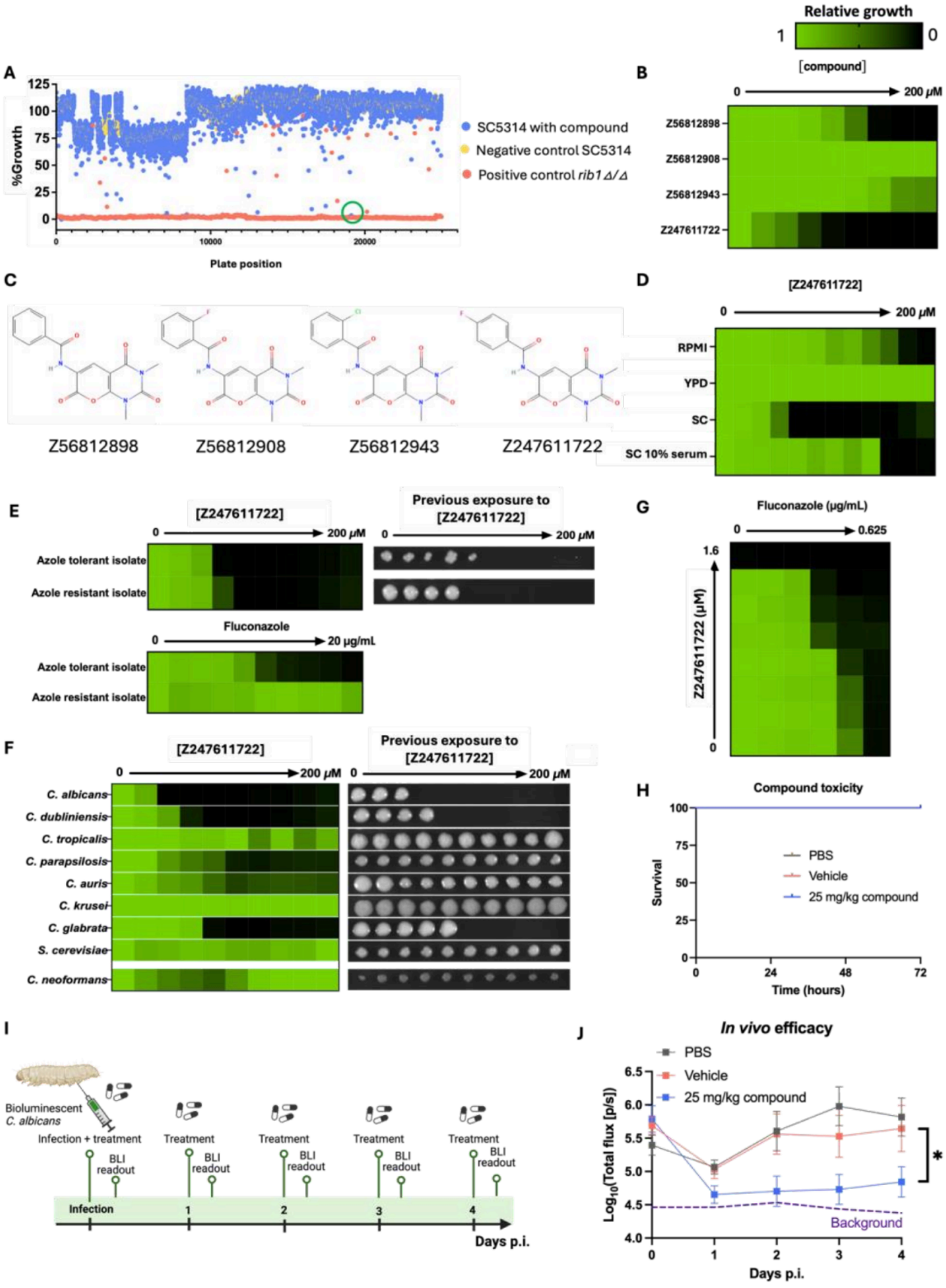


Figure 1

Z247611722 demonstrates fungicidal activity against multiple Candida species and fluconazole-tolerant and -resistant strains. (A) Result of the high-throughput screen. A total of 20,000 compounds were screened for their ability to inhibit C. albicans growth. The screening was conducted by adding 50 μM of each compound to SC5314, which was grown in LoFlo medium at 30°C. Absorbance was measured after 24 h, and the percent growth was calculated by normalizing the absorbance of the wells with compound to the wild-type controls. (B) Compound analogs were cultivated in a two-fold BDA, and growth was measured after 24 h. Technical repeats were averaged, and the relative growth was depicted (see colour bar). (C) Structures of the hit compound Z56812898 and analogs. (D) Two-fold BDA assays were performed in different media. Growth was measured after 48 h. Technical repeats were averaged, and the relative growth was depicted. (E) The bioactivity of compound Z247611722 was assessed against an azole-tolerant (CaCi-2) and an azole-resistant strain (CaCi-17). Technical repeats were averaged, and the relative growth was depicted. The absorbance was measured after 48 h. Technical repeats were averaged, and the relative growth was depicted. After 72 h, the BDA plates were stamped on a drug-free YPD plate to assess cidality of the compounds. The plates were grown for 48 h at 30°C prior to imaging. (F) The antifungal activity of compound Z247611722 was tested against a panel of yeast species. The absorbance was measured after 48 h, except for C. neoformans, which was grown for 72 h. Technical repeats were averaged, and the relative growth was depicted. After 72 h, the BDA plates were stamped on a drug-free YPD plate to assess cidality of the compounds, as described in panel E. (G) A checkerboard assay was performed to assess the interaction between Z247611722 and fluconazole. The absorbance at 600 nm was measured after 48 h. (H) Survival curve of G. mellonella injected with either 25 mg/kg compound, vehicle (4.88% DMSO), or PBS. The larvae were monitored for 72 h. Ten 6^{th}-instar larvae of 300 ± 50 mg were randomly selected in each group. The mean ± standard error of the mean (SEM) is shown. (I) Overview of the set-up of the G. mellonella treatment efficacy experiment. (J) BLI signal of larvae infected with 5 x 10^4 cells/larvae up to 4 days post-infection (p.i.). larvae were either treated with compound or received the vehicle or PBS control. Ten 6^{th}-instar larvae of 300 ± 50 mg were randomly selected in each group. Larvae that died during the experiment were excluded from BLI statistical analyses but the final recorded values before death were retained in the graph to minimize visual survival bias. In vivo, BLI data was $\log_{10}$ transformed and the mean ± SEM is shown. Statistical analysis was performed using mixed-effect analysis. *, $p < 0.05$.

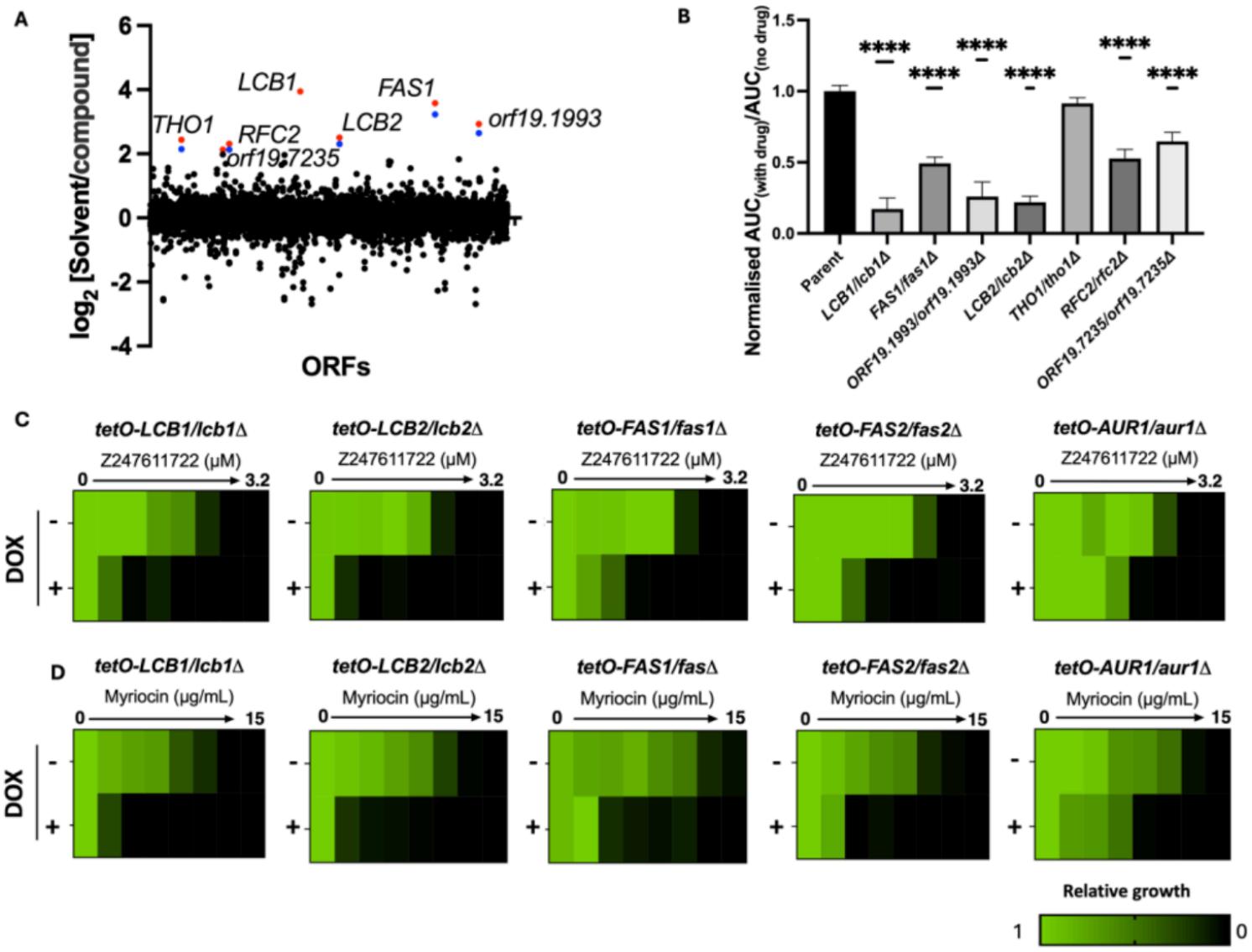


Figure 2

Chemical-genetic profiling suggests Z247611722 targets the sphingolipid biosynthetic pathway (A) C. albicans HIP profile of compound Z247611722. A double-barcoded heterozygous deletion mutant library was cultured in the presence and absence of 1.5 μM Z247611722. Genomic DNA was extracted and barcodes were amplified via PCR and subsequently pooled for sequencing to evaluate the abundance of every heterozygous strain. Strains with a solvent/drug $\log_2$ ratio greater than 2 were considered hypersensitive and are shown in red (upstream barcode) or blue (downstream barcode). (B) Hits from panel A were validated in a growth curve assay with the corresponding heterozygous mutants. Strains were cultured in SC medium for 24h at 30°C. The area under the curve (AUC) was calculated, and the ratio of AUC with compound compared to without compound was normalized to the parental control. The mean with standard deviation (s.d.) of three technical repeats is shown, and statistical analysis was performed using one-way ANOVA with Bonferroni correction. ****, $P < 0.0001$. (C-D) Mutants from the GRACE collection involved in lipid biosynthesis pathways were tested for susceptibility to Z247611722 (C) or myriocin (D) in the presence and absence of DOX. Only the most hypersensitive hits are shown

(see Supplementary Figure 3 for all mutants tested). Growth was normalized to compound-free controls (see colour bar).

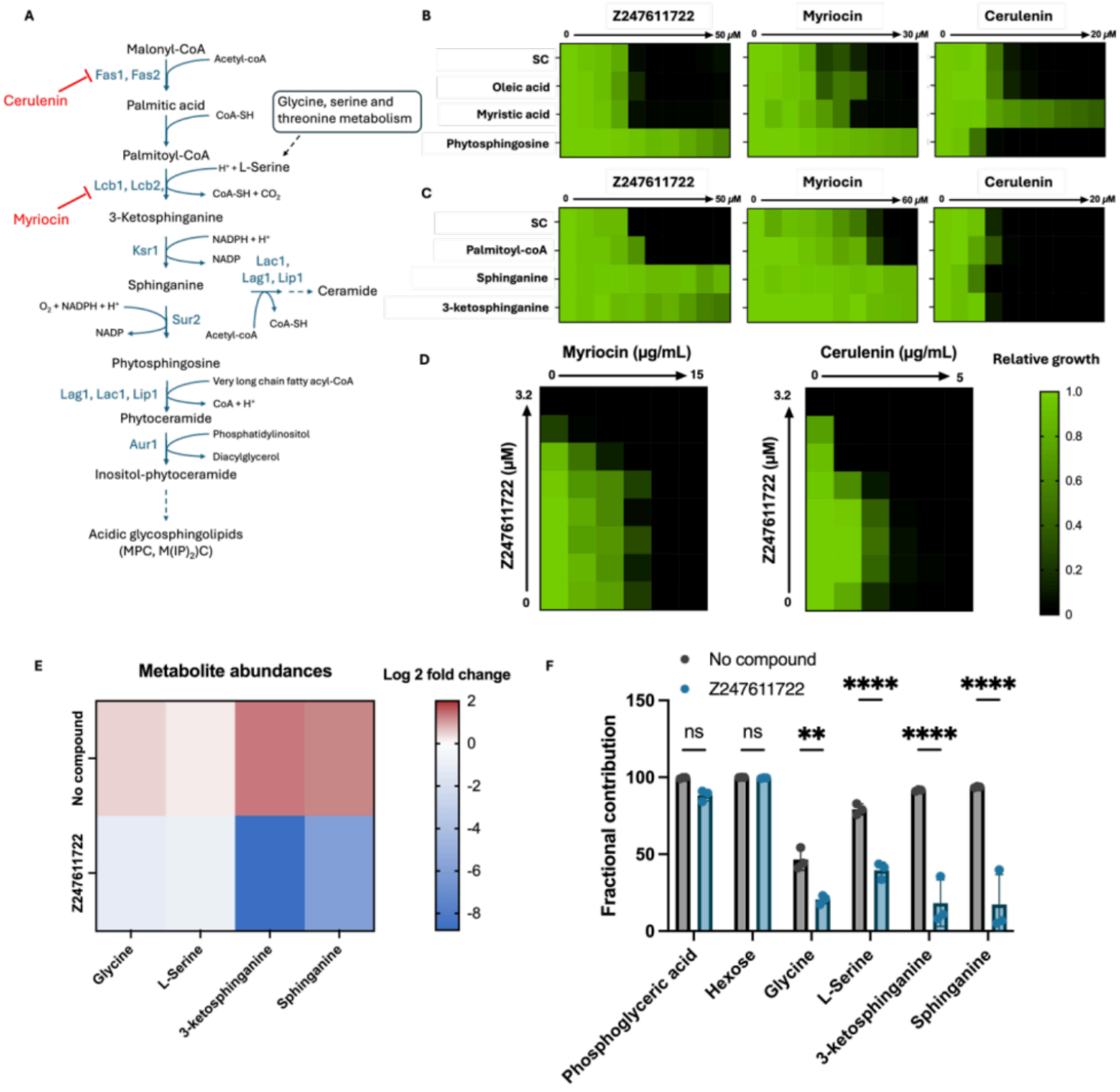


Figure 3

Z247611722 inhibits sphingolipid biosynthesis. (A) Simplified schematic of sphingolipid biosynthesis pathway in yeasts. (B-C) Two-fold compound dilutions of Z247611722, myriocin, and cerulenin were prepared in the presence of (B) oleic acid (0,05%), myristic acid (0,05%), and phytosphingosine (10 µM) or (C) palmitoyl-CoA (10 µM), sphinganine (10 µM), and 3-ketosphinganine (10 µM). Absorbance at 600

nm was measured after 48 h of incubation at 30 °C, and the relative growth was plotted (see colour bar). (D) Checkerboard assays were conducted with Z247611722 in combination with myriocin or cerulenin. The absorbance at 600 nm was measured after 48 h of incubation. Data are shown as averaged technical repeats, and the relative growth is depicted (see colour bar). (E) The abundance of glycine, L-serine, 3-ketosphinganine, and sphinganine was measured in C. albicans samples with compound and a vehicle control. The results were normalized to the OD_{600}, median-centered, and $\log_2$ transformed. The averages of three technical repeats are shown. Increased abundance is displayed in red and decreased abundance in blue. (F) The fractional contribution of U-$^{13}C_6$-glucose tracing in different metabolites is shown. The bars show the average of three repeats, and statistical analysis was performed using 2-way ANOVA with Bonferroni's multiple comparisons tests. **, P < 0.01, ****, P < 0.0001.

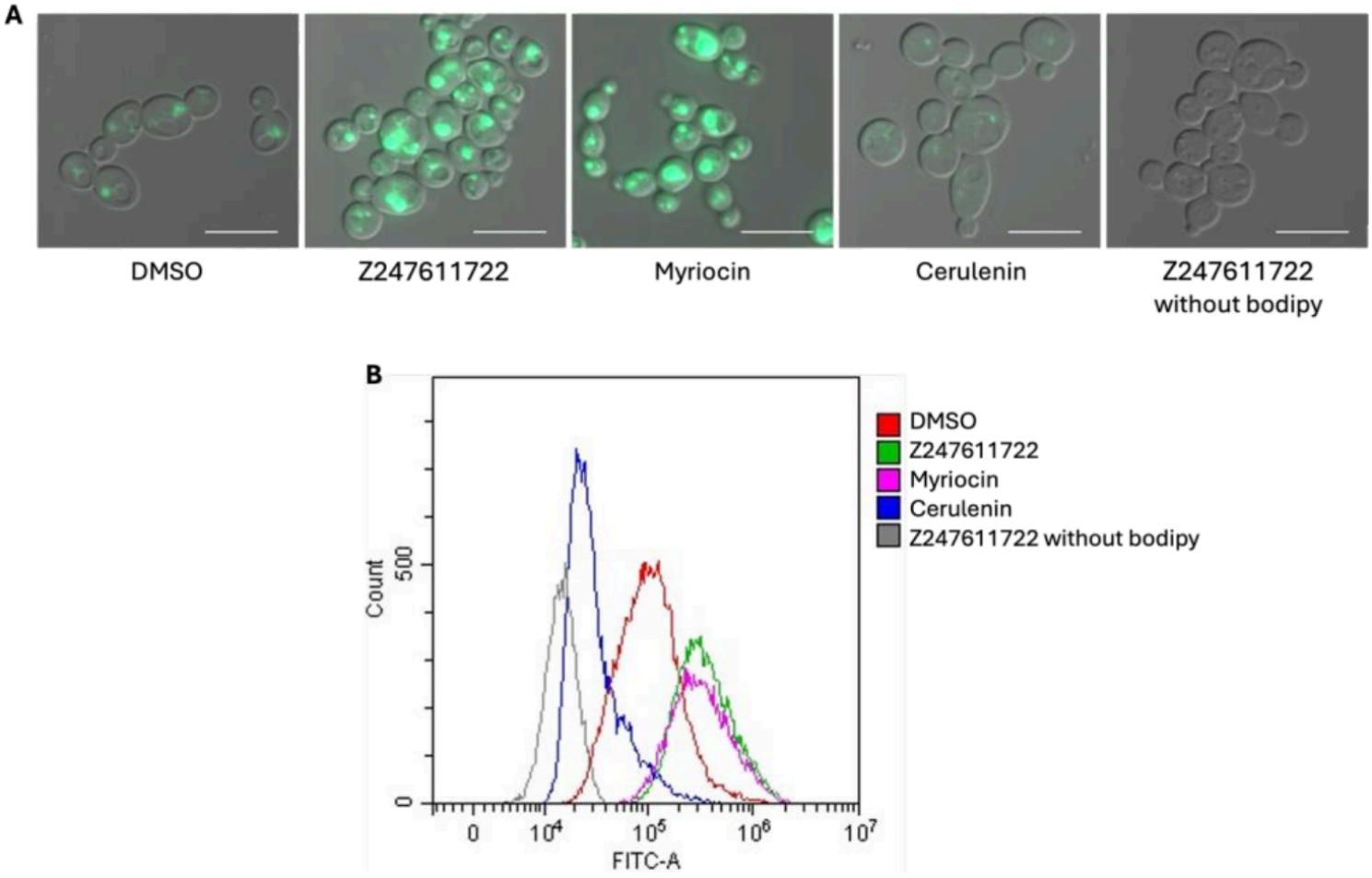


Figure 4

Z247611722 induces lipid droplets in a similar manner to myriocin. (A) C. albicans was cultured in the presence of 1.5 μM Z247611722, 1 μg/μL myriocin, 5 μg/μL cerulenin, or vehicle (DMSO) for 4 h at 30 °C. Cells were stained with 1 μg/mL BODIPY 493/503 to stain the lipid droplets and were subsequently washed three times with PBS. Visualization was performed on a Zeiss Axio Imager.MI using ×100 magnification with differential interference contrast (DIC) and an enhanced green fluorescent protein fluorescence filter. The white scale bars represent 10 μm. (B) The amount of relative lipid droplets of

each treatment was quantified using flow cytometry. The relative fluorescence intensity of the incorporated BODIPY dye was analyzed and plotted. Cells were gated using forward and side scatter to isolate the main population and remove debris. At least 10,000 events were measured in each condition.

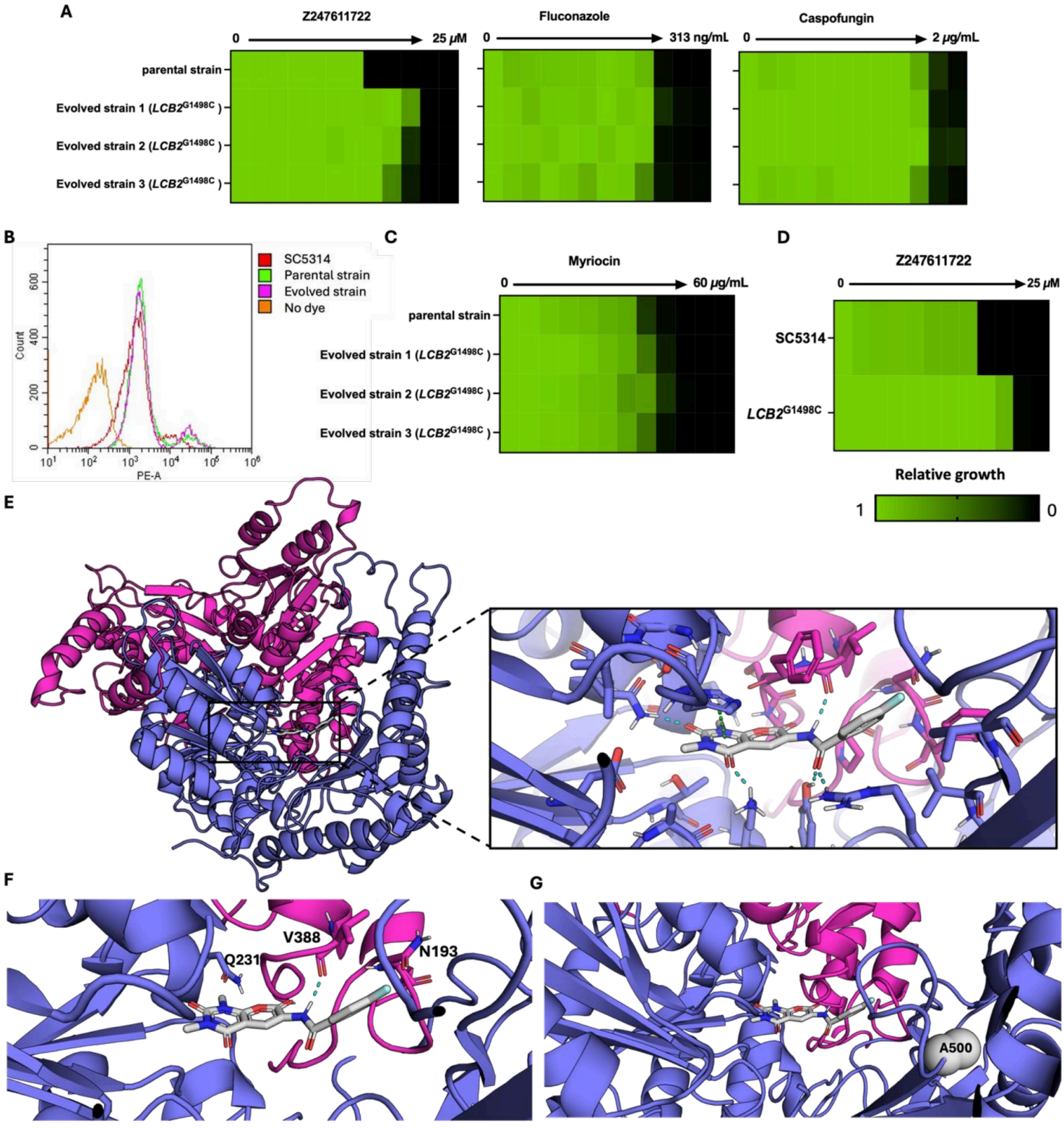


Figure 5

An alanine-to-proline substitution in Lcb2 confers resistance to Z247611722. (A) Resistant strains were evolved in a mdr1D/D cdr1D/D cdr2D/D flu1D/D background strain. The susceptibility of these strains was assessed in two-fold BDAs by measuring the absorbance at 600 nm after 48 h at 30 °C (see colour bar). (B) A possible increase in efflux of the resistant strains was evaluated using Nile red dye. At least 1000 cells were assessed via flow cytometry, and the relative fluorescence intensity is displayed in the histogram. (C) The susceptibility of the strains towards myriocin was evaluated in a two-fold BDA as described in A. (D) A heterozygous guanine to cytosine SNP was introduced in the SC5314 background, and the susceptibility was compared in a two-fold BDA towards Z247611722. The average of three independently transformed strains with two technical repeats is shown. (E) Proposed binding pose of the compound in C. albicans SPT. Lcb1 colored in purple, Lcb2 colored in blue, cyan dashed lines represent hydrogen bonds, green dashed lines represent π–π stacking. (F) Non-conserved residues of C. albicans compared to G. mellonella, S. cerevisiae, and Homo sapiens. Lcb1 is colored in purple, and Lcb2 is colored in blue. (G) Location of residue A500 in C. albicans. Lcb1 is colored in purple, and Lcb2 is colored in blue.

Supplementary Files

This is a list of supplementary files associated with this preprint. Click to download.

- Supplementarytablesandfigures.docx